Clusters of polyhedra in spherical confinement

Erin G. Teich[a], Greg van Anders[b], Daphne Klotsa[b,1], Julia Dshemuchadse[b], and Sharon C. Glotzer[a,b,c,d,2]

[a]Applied Physics Program, University of Michigan, Ann Arbor, MI 48109; [b]Department of Chemical Engineering, University of Michigan, Ann Arbor, MI 48109; [c]Department of Materials Science and Engineering, University of Michigan, Ann Arbor, MI 48109; and [d]Biointerfaces Institute, University of Michigan, Ann Arbor, MI 48109

Contributed by Sharon C. Glotzer, December 21, 2015 (sent for review December 1, 2015; reviewed by Randall D. Kamien and Jean Taylor)

Dense particle packing in a confining volume remains a rich, largely unexplored problem, despite applications in blood clotting, plasmonics, industrial packaging and transport, colloidal molecule design, and information storage. Here, we report densest found clusters of the Platonic solids in spherical confinement, for up to $N = 60$ constituent polyhedral particles. We examine the interplay between anisotropic particle shape and isotropic 3D confinement. Densest clusters exhibit a wide variety of symmetry point groups and form in up to three layers at higher N. For many N values, icosahedra and dodecahedra form clusters that resemble sphere clusters. These common structures are layers of optimal spherical codes in most cases, a surprising fact given the significant faceting of the icosahedron and dodecahedron. We also investigate cluster density as a function of N for each particle shape. We find that, in contrast to what happens in bulk, polyhedra often pack less densely than spheres. We also find especially dense clusters at so-called magic numbers of constituent particles. Our results showcase the structural diversity and experimental utility of families of solutions to the packing in confinement problem.

clusters | confinement | packing | colloids | nanoparticles

Phenomena as diverse as crowding in the cell (1, 2), DNA packaging in cell nuclei and virus capsids (3, 4), the growth of cellular aggregates (5), biological pattern formation (6), blood clotting (7), efficient manufacturing and transport, the planning and design of cellular networks (8), and efficient food and pharmaceutical packaging and transport (9) are related to the optimization problem of packing objects of a specified shape as densely as possible within a confining geometry, or packing in confinement. Packing in confinement is also a laboratory technique used to produce particle aggregates with consistent structure. These aggregates may serve as building blocks (or "colloidal molecules") in hierarchical structures (10, 11), information storage units (12), or drug delivery capsules (13). Experiments concerning cluster formation via spherical droplet confinement (13–20) are of special interest here. Droplets are typically either oil-in-water or water-in-oil emulsions, and particle aggregation is induced via the evaporation of the droplet solvent. Clusters may be hollow [in which case they are termed "colloidosomes" (13)] or filled, depending on the formation protocol, and may contain a few (15) to a few billion (14) particles. Clusters of several metallic nanoparticles are especially intriguing given their ability to support surface plasmon modes over a range of frequencies (21). The subwavelength scale of these clusters means that their optical response is highly dependent on their specific geometry (22). Consequently, control over their structure enables control over their optical properties, with implications for cloaking (23), chemical sensing (24), imaging (25), nonlinear optics (26), and the creation of so-called metafluids (27–29), among a host of other applications (30). Recent work on plasmonic nanoclusters of faceted particles including nanocubes (31), nanoprisms (32), and nanooctahedra (33) introduces an additional means by which to tailor optical response.

While some theoretical studies have addressed the confinement of anisotropic particles in one or two dimensions (34–38), a majority have focused on the confinement of spherical particles in one, two, and three dimensions (8, 19, 39–50). There have also been studies of 2D packings of circles, ellipses, and convex polygons (9, 51–55). However, to our knowledge, only a handful of studies have addressed 3D dense packings of anisotropic particles inside a container. Of these, almost all pertain to packings of ellipsoids inside rectangular, spherical, or ellipsoidal containers (56–58), and only one investigates packings of polyhedral particles inside a container (59). In that case, the authors used a numerical algorithm (generalizable to any number of dimensions) to generate densest packings of $N = (1 - 20)$ cubes inside a sphere.

In contrast, the bulk densest packing of anisotropic bodies has been thoroughly investigated in 3D Euclidean space (60–65). This work has revealed insight into the interplay between packing structure, particle shape, and particle environment. Understanding the parallel interplay between shape and structure in confined geometries is both of fundamental interest and of relevance to the host of biological and materials applications already mentioned.

Here, we use Monte Carlo simulations to explore dense packings of an entire shape family, the Platonic solids, inside a sphere. The Platonic solids are a family of five regular convex polyhedra: the tetrahedron, cube, octahedron, dodecahedron, and icosahedron. Of these, all but the icosahedron are readily synthesized at nanometer scales, micrometer scales, or both (see, for example, refs. 35 and 66–76). For each polyhedron we generate and analyze dense clusters consisting of $N = (4 - 60)$ constituent particles. We also generate dense clusters of hard spheres for the purposes of comparison.

We find, for many N values, that the icosahedra and dodecahedra pack into clusters that resemble sphere clusters, and consequently form layers of optimal spherical codes. For a few low values of N the packings of octahedra and cubes also resemble sphere clusters. Clusters of tetrahedra do not. Our results, in contrast to those for densest packings in infinite space where particle shape significantly affects packing structure (60, 62–64),

Significance

What is the best way to pack objects into a container? This simple question, one that is relevant to everyday life, biology, and nanoscience, is easy to state but surprisingly difficult to answer. Here, we use computational methods to determine dense packings of a set of polyhedra inside a sphere, for up to 60 constituent packers. Our dense packings display a wide variety of symmetries and structures, and indicate that the presence of the spherical container suppresses packing effects due to polyhedral shape. Our results have implications for a range of biological phenomena and experimental applications, including blood clotting, cell aggregation, drug delivery, colloidal engineering, and the creation of metamaterials.

Author contributions: E.G.T., G.v.A., D.K., and S.C.G. designed research; E.G.T., G.v.A., and S.C.G. performed research; E.G.T. and G.v.A. contributed new reagents/analytic tools; G.v.A. and S.C.G. supervised research; E.G.T., G.v.A., J.D., and S.C.G. analyzed data; and E.G.T., G.v.A., D.K., J.D., and S.C.G. wrote the paper.

Reviewers: R.D.K., University of Pennsylvania; and J.T., Courant Institute, New York University.

The authors declare no conflict of interest.

[1]Present address: Department of Applied Physical Sciences, University of North Carolina, Chapel Hill, NC 27599.

[2]To whom correspondence should be addressed. Email: sglotzer@umich.edu.

This article contains supporting information online at www.pnas.org/lookup/suppl/doi:10.1073/pnas.1524875113/-/DCSupplemental.

suggest that the presence of the container suppresses the packing influence of particle shape at the range of N studied. Spherical confinement provides a means by which to impose certain symmetries on anisotropic particles that otherwise might not pack like spheres. The imposed structures are a set of dense motifs that are robust against changes in particle shape. This result has implications for experimental applications in which the fabrication of highly spherical particles is difficult or undesirable, as in the case of several plasmonic applications mentioned earlier (31, 33, 77).

We also examine cluster structure and density as they vary across each individual set of densest found packings and find a wide variety of cluster symmetries as N varies. We note that in a spherical container, in contrast to the situation in infinite space described by Ulam's conjecture, spheres are not the worst packers of all convex bodies at small N. We additionally find that certain values of N, so-called magic numbers (78–81), correspond to especially high cluster densities of a given particle shape. These magic numbers, however, do not correspond to any particular cluster symmetry, indicating that especially dense clusters exist with a variety of symmetries and structures. Many of these structures are unachievable with densely packed spheres and are stabilized by a variety of contact types. They will be of interest to experimentalists who use clusters for plasmonics and other colloidal molecule applications.

Materials and Methods

Simulation. To generate finite dense packings of N identical polyhedra and spheres in spherical confinement, we use isobaric Monte Carlo simulations and specialized particle overlap checks with respect to a spherical container. We run 50 independent compression simulations at every (shape, N) state point, calculate the density for each of the resultant clusters via $\phi_{circ} \equiv NV_p/V_{circ}$, and choose the densest for further analysis. V_p is the volume of a single particle and V_{circ} is the volume of the container.

For consistency, all particles are scaled such that they have equal circumscribing sphere radii. The particle positions and orientations evolve during the simulation according to a trial-move update scheme, wherein particles are chosen randomly and then translated or rotated (in the case of nonspherical particles) by a random amount. Although this decoupling of particle rotation and translation is not necessary, we choose it so that we can tune the size of each move type independently as detailed below. In tight confinement, translation possibilities for a particle may be more limited than rotation possibilities (or vice versa), so independent tuning enables an efficient and agnostic sampling of phase space. Moves are rejected if they result in any particle overlaps or the presence of a portion of any particle outside the spherical container. Due to their faceting, polyhedra are fully encased in the container if all their vertices are inside the container. Spheres are fully encased in the container as long as their radial distance from the container center remains within a small tolerance of $(R_{circ} - R)$, where R_{circ} is the container radius and R is the particle radius.

We induce increasing spherical confinement by raising dimensionless pressure exponentially from a minimum value of 0.1 to a maximum value of 500. Dimensionless pressure is defined here as $p^* \equiv \beta p l^3$, where p is pressure and $l = R$ is the characteristic length scale in our systems. It is the particle radius for simulations involving spheres, whereas for simulations involving polyhedra it is the radius of their circumscribing sphere. The system is allowed to equilibrate for 1,000 Monte Carlo sweeps between pressure jumps. The total compression occurs over 10^7 sweeps. Particle translation and rotation (for nonspherical particles) are equally likely to occur when a particle move is chosen, while container resize moves occur with a probability equal to $1/(N+1)$. During the run, simulation parameters are tuned such that particle translation, particle rotation, and container resize acceptance rates are ~0.2. (We found an acceptance rate of 0.2 to be near optimal in similar Monte Carlo implementations, so we adopted this as a convention.) Container shrinking moves are always accepted provided that they do not cause any particle overlaps and that confinement is maintained, whereas container expansion moves are accepted with a probability

$$P_{o\to n} = \exp[-\beta p(V_n - V_o) + N\log(V_n/V_o)], \quad [1]$$

where V_n is the new container volume and V_o is the old container volume (82). Container resizing consists of rescaling the container radius and is accompanied by identical rescaling of all particle positions with respect to the container center.

Fig. 1 summarizes our simulation method. Fig. 1*A* displays the shapes studied, Fig. 1*B* shows a sample trajectory of cluster formation via our compression scheme, and Fig. 1*C* includes snapshots of the cluster at indicated pressures.

Analysis. We use the isoperimetric quotient (IQ) to characterize particle sphericity, as in previous studies (83). $IQ \equiv 36\pi V^2/S^3$, where V is polyhedron volume and S is surface area. For spheres, $IQ = 1$, and for all other polyhedra, $0 < IQ < 1$ (84).

To decompose each cluster into layers, we use the DBSCAN clustering algorithm (85) in the scikit-learn Python module (86). DBSCAN operates on the set of radial distances from the cluster centroid to all particle centroids.

We compute bond order parameters (87) and use them to build associated shape descriptors (88) for each cluster and each cluster layer in the following manner. For a given l, the bond order parameter for a set of N points constituting cluster i is

$$Q_l^i \equiv \left[\frac{4\pi}{2l+1}\sum_{m=-l}^{l}\left|\frac{1}{N}\sum_{j=1}^{N}Y_l^m\left(\vec{r}_j\right)\right|^2\right]^{1/2}, \quad [2]$$

where $\vec{r}_j$ is the vector pointing from a reference point to point j, and Y_l^m is the spherical harmonic associated with angular momentum number l and magnetic quantum number m. We use the centroid of cluster i as our reference point.

Point clusters of a given symmetry have well-defined values of Q_l for various l. More generally, a vector of these order parameters at multiple values of l, $\{l_1, l_2 \ldots l_n\}$, acts as a signature for a particular distribution of points over the surface of a sphere. This vector constitutes a shape descriptor (88) characterizing a particular cluster i:

$$\vec{Q}_i = \langle Q_{l_1}^i, Q_{l_2}^i, \ldots Q_{l_n}^i \rangle, \quad [3]$$

where $\vec{Q}_i$ lies in n-dimensional space. We use the set of l = (2, 3, …12) to calculate this vector. Because the spherical harmonics are functions of the

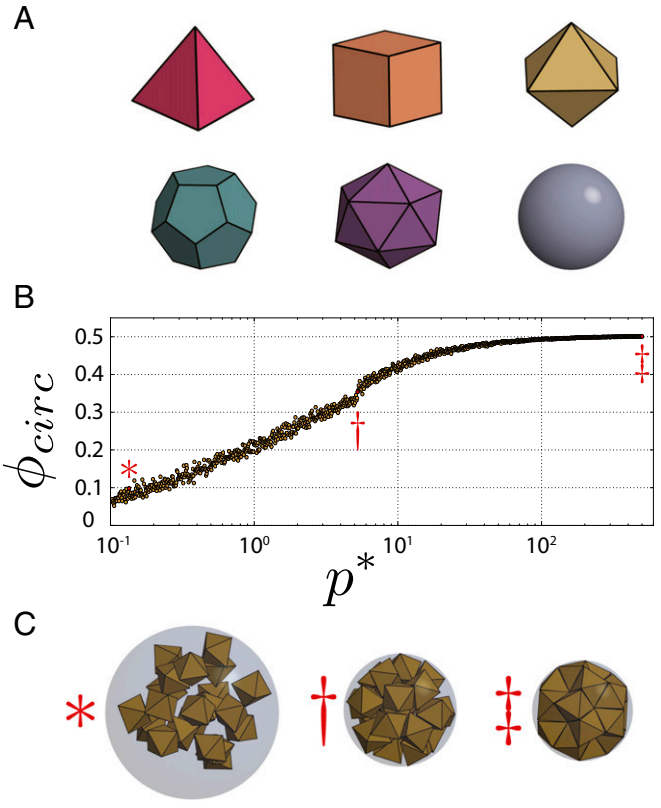

Fig. 1. Overview of our methods. (*A*) The particle shapes studied: the Platonic solids and the sphere. (*B*) The evolution of the densest found 21-octahedron cluster via NPT compression in a spherical container. p^* is the dimensionless pressure imposed on the system, and ϕ_{circ} is the density of the cluster. (*C*) Cluster images at $p^* = 0.135$, $p^* = 5.246$, and $p^* = 500$.

azimuthal and polar angles only, $\vec{Q}_i$ contains angular, rather than radial, information about the set of points.

To evaluate how well two different point configurations i and j match, we use the following quantity:

$$M_{dist}(i,j) \equiv 1 - \frac{|\vec{Q}_i - \vec{Q}_j|}{\sqrt{|\vec{Q}_i|^2 + |\vec{Q}_j|^2}}, \quad [4]$$

effectively a normalized measure of the distance between two Q-vectors (88). $M_{dist}(i,j)$ is 1 when $\vec{Q}_i = \vec{Q}_j$ and 0 when $\vec{Q}_i$ is perpendicular to $\vec{Q}_j$. We take $M_{dist}(i,j) > 0.88$ to be the quantitative indicator that sets of points i and j are similar, based on comparisons to the root-mean-squared distance between a set i of random points on the surface of the unit sphere and its subsequent perturbation to set j. See the *SI Appendix* for more details.

Results

All dense clusters are layered structures with maximally three shells at higher N. The layering is less distinct in clusters of the least spherical particles, namely the cubes and tetrahedra. Our tuned DBSCAN parameters delineate cluster layers in nearly all cases, but we fail to detect distinct layering for one cluster of cubes ($N = 39$) and for 14 clusters of tetrahedra ($N = 45,46,49-60$). Although these clusters consist of particles at a range of radial distances from each cluster center, the radial distances are not well-separated enough to be grouped into separate layers by DBSCAN.

Comparison with Sphere Clusters. We first compare our results for the densest found clusters of the Platonic solids with those of spheres. To measure similarity, we use M_{dist}^{sph}, given by Eq. **4** when i is the set of polyhedron centroids for a given cluster of polyhedra and j is the set of particle centroids for the corresponding sphere cluster. Fig. 2*A* shows a scatter plot of values of M_{dist}^{sph} for every densest found cluster as a function of the IQ of the constituent particle shape. Average values $\langle M_{dist}^{sph} \rangle$, computed across the set of all densest found clusters of each Platonic solid, are also marked in Fig. 2*A* with an image of the associated particle. Plots of M_{dist}^{sph} as a function of N for all Platonic solids are shown in the *SI Appendix*.

Given the similarity criterion $M_{dist}^{sph} > 0.88$ (marked by a black horizontal line in Fig. 2*A*), we find that the number of clusters that are similar to sphere clusters is quite high for the icosahedron (the most spherical Platonic solid) and trends downward as the IQ of the particle shape decreases. Of the 57 densest clusters found for each particle shape, 44 clusters of icosahedra, 20 clusters of dodecahedra, 2 clusters of octahedra, 2 clusters of cubes, and no clusters of tetrahedra are structurally similar to their corresponding cluster of spheres. $\langle M_{dist}^{sph} \rangle$ also trends downward as IQ decreases.

Comparison with Optimal Spherical Codes. The dense sphere clusters consist of layers whose configurations map to optimal spherical codes for a majority of cases. A spherical code, or finite set of points on the surface of a sphere, can be characterized by the minimal angle between vectors pointing from the center of the sphere to any two of the points. Optimal spherical codes are ones for which this minimal angle, which corresponds to the smallest distance between any two of the points, is maximized (89, 90). Given a point radius (i.e., turning these points into circles), the optimal spherical code at N maps to the arrangement of N circles on a sphere such that they fit on its surface at minimal sphere radius. Optimal spherical codes are therefore a way of packing spherical particles such that their configuration within a cluster layer is spherical but still tightly packed. These motifs accordingly dominate in the dense sphere clusters, from which we demand that the particles both pack densely and fit inside a sphere.

The relationship between densest packings within a container and optimal spherical codes was previously addressed by Hopkins et al. (90, 91). They defined the N-specific densest local packing (DLP) problem, equivalent to finding the densest packing of spheres within a spherical container given that one additional sphere must always be at the center of the container. Hopkins et al. (90) proved that every solution to the optimal spherical code problem is also a solution to the DLP problem for $1 \le R \le \tau$, where R is the greatest distance from the container center to the center of any sphere and τ is the golden ratio. They also found solutions to the DLP problem for selected values of N up to $N = 1,054$ and noted that the majority of their solutions maximized the number of spheres in the surface layer according to the optimal spherical code at the relevant container radius (91).

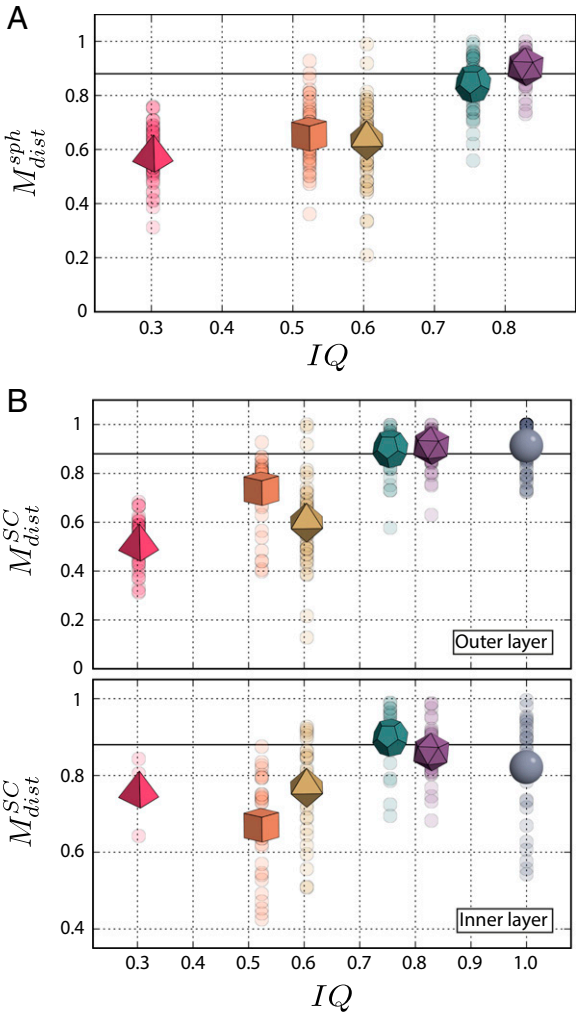

Fig. 2. Comparison of (*A*) densest found clusters of the Platonic solids to densest found clusters of spheres, indicated by M_{dist}^{sph}, and (*B*) the outermost and next inner layers of densest found clusters of the Platonic solids and spheres to optimal spherical codes, indicated by M_{dist}^{SC}. M_{dist}^{SC} for any layer is only plotted when $N_{layer} \ge 4$. Values of M_{dist} for all clusters and cluster layers are plotted as a function of the isoperimetric quotient (IQ) of the constituent particle shape. Clusters whose value of M_{dist} lies above 0.88, indicated by a horizontal line in each figure, are deemed similar to their corresponding cluster of spheres or optimal spherical code. Average values $\langle M_{dist} \rangle$, computed across the set of all densest found clusters or relevant cluster layers for each particle shape, are marked with an image of the associated shape. The more spherical polyhedra (icosahedra and dodecahedra) form clusters that increasingly resemble those of spheres, and a majority of sphere, icosahedron, and dodecahedron cluster layers match optimal spherical codes.

Here, we expand upon those observations and find that optimal spherical codes are prevalent motifs in solutions to a more general problem, one in which there is no particle fixed at the center of the container and the packing particles are not just spheres but faceted particles as well.

To determine the similarity between cluster layers and optimal spherical codes, we use M_{dist}^{SC}, given by Eq. **4** when i is the set of particle centroids in a particular cluster layer and j is the optimal spherical code at equal N_{layer}. We use conjectured optimal spherical codes found in ref. 92. The criterion for similarity is again $M_{dist}^{SC} > 0.88$.

Fig. 2*B* shows scatter plots of values of M_{dist}^{SC}, both for the outermost layer and the next inner layer of every densest cluster found, as a function of the IQ of the constituent particle shape. M_{dist}^{SC} for any layer is only plotted when $N_{layer} \geq 4$. At higher N, there is also a third (innermost) layer, but at the particle numbers we studied this third layer is just a single central particle and is not included in the figure. Average values $\langle M_{dist}^{SC} \rangle$ for each layer, computed across the set of all relevant layers of each particle shape, are also marked in Fig. 2*B* with an image of the associated particle. Table 1 tabulates this data. Plots of M_{dist}^{SC} as a function of N for all particle shapes are given in the *SI Appendix*.

Optimal spherical code motifs constitute the majority of layers for sphere, icosahedron, and dodecahedron clusters, and even appear in layers of the octahedron and cube clusters. Additionally, $\langle M_{dist}^{SC} \rangle > 0.88$ (marked by black horizontal lines in Fig. 2*B*) for the outer layers of the sphere, icosahedron, and dodecahedron clusters and the inner layer of the dodecahedron cluster, indicating that these layers are, on average, optimal spherical codes. This is far from the case for the clusters of octahedra, cubes, and tetrahedra.

Given the wealth of studies showing that bulk dense packing is sensitive to minute differences in particle shape (e.g., refs. 65, 93, and 94), it is interesting that in spherical confinement icosahedra and dodecahedra pack like spheres. This is noteworthy because of a combination of two facts. First, icosahedra and dodecahedra are dual to each other (i.e., everywhere an icosahedron has a face, a dodecahedron has a vertex, and vice versa). Second, polyhedra make contact with the spherical container only at their vertices. These two facts would lead us to expect that icosahedra would arrange themselves differently from dodecahedra at the surface of the container to accommodate the "opposite" location of their vertices. However, what we observe instead is that the layered spherical code structures that occur for sphere packing are robust against changes in particle shape.

Common Cluster Structures. Similarity to sphere clusters and optimal spherical codes produces a class of common structures formed by different particle types at specific values of N. Values of N for which more than two particle types share a common cluster geometry, as well as the respective cluster structure, are shown in Fig. 3. More common structures could be listed here if we relax our M_{dist}^{sph} criterion; the current set represents a sample based on our cutoff $M_{dist}^{sph} > 0.88$. For most of these values of N, common structures are shared by clusters of spheres, icosahedra, and dodecahedra. Layers of these similar clusters are optimal spherical codes, indicated by $M_{dist}^{SC} > 0.88$, in all but six cases.

That these common motifs emerge simply from the spherical confinement of particles as nonspherical as dodecahedra, and in some cases even octahedra and cubes, is a result with intriguing experimental implications. Common configurations are resistant to significant deviations from spherical particle shape, meaning that they may be ideal target structures for the self-assembly of imperfectly spherical colloidal particles or faceted metallic nanoparticles. We will explore this idea further in the *Conclusions*.

Table 1. Outermost and next inner cluster layers as optimal spherical codes

Particle shape	Outer: SC (total)	$\langle M_{dist}^{SC} \rangle$	Inner: SC (total)	$\langle M_{dist}^{SC} \rangle$
Sphere	36 (57)	0.91	14 (30)	0.82
Icosahedron	43 (57)	0.91	14 (30)	0.86
Dodecahedron	42 (57)	0.90	20 (30)	0.90
Octahedron	3 (57)	0.60	6 (32)	0.77
Cube	1 (57)	0.74	0 (35)	0.67
Tetrahedron	0 (57)	0.52	0 (3)	0.76

Numbers corresponding to SC (total) are the number of layers that are deemed similar to optimal spherical codes (SC) for each particle shape, followed in parentheses by the total number of layers for which $N_{layer} \geq 4$. $\langle M_{dist}^{SC} \rangle$ is an average taken over each set of layers counted in the parentheses.

Cluster Symmetry and Density. We next examine the relationship between symmetry and density of the dense packings as a function of N. Fig. 4 shows both of these cluster properties simultaneously: the respective crystal systems of the symmetry point groups of the outermost cluster layers are shown as vertical bars of color overlaid on plots of the cluster density ϕ_{circ} as a function of N. The crystal systems of the outermost layers are also tallied in Table 2. Point groups were determined by eye for all clusters.

Density profiles are similar in behavior for all particle shapes: density increases sharply with N at low values of N, as the densest clusters gain enough particles to be approximately spherical, and then more gradually grows as N increases. We expect ϕ_{circ} to approach the bulk densest packing fraction for each particle shape as N goes to infinity, although at $N = 60$ the density is still far from its bulk value in all cases. Cluster symmetry, however, varies widely across N for all particle shapes.

The set of conjectured optimal spherical codes displays a wide variety of point groups (95, 96), and it is thus unsurprising that the layers of the sphere, icosahedron, and dodecahedron clusters also have a variety of symmetries as N varies, at least when they match optimal spherical codes. Within the set of sphere, icosahedron, and dodecahedron clusters, a majority of clusters have nontriclinic point groups, and these point groups are spread widely across 10 crystal systems.

It is significant, however, that even those cluster layers that do not map to optimal spherical codes display a variety of symmetries. These include the icosahedron and dodecahedron layers for which $M_{dist}^{SC} \leq 0.88$, as well as the majority of octahedron, cube, and tetrahedron cluster layers. In many cases, irrespective of the anisotropic particle shape, the requirement of high density and cluster sphericity imposed by the container selects for symmetric clusters.

Comparison with Bulk Packing Behavior. As an interesting aside, Ulam conjectured that spheres pack less densely than all other convex solids in infinite space (97). The n-dimensional analog of Ulam's conjecture is violated in Euclidean spaces for $n = 2,4,5,6,7,8,$ and 24 (98), but in three dimensions it has been shown that spheres pack less densely than any other infinitesimal centrosymmetric convex shape deformation (98). It is not known whether in three dimensions spheres continue to be pesimal packers in confinement. We find that for a majority of lower N values, spheres pack inside a spherical container more densely than one or more Platonic solids. In fact, at $N = (4-9)$, the sphere cluster has the highest value of ϕ_{circ}. Spheres are only the worst packers for $N = (26,29,31-33,35)$. We believe these results can be explained by considering the volume occupied by the particles in a spherical shell just below the container surface. A single spherical particle necessarily packs more densely than a convex faceted particle near the surface of the container, due to the fact that the faceted particle may touch the container only at its vertices. This density gain by spherical particle packing is a surface effect and matters less and less as N increases. At small values of N, however, it enables spheres to pack more densely than the various Platonic solids inside a spherical container, in contrast to what Ulam's conjecture asserts for infinite space.

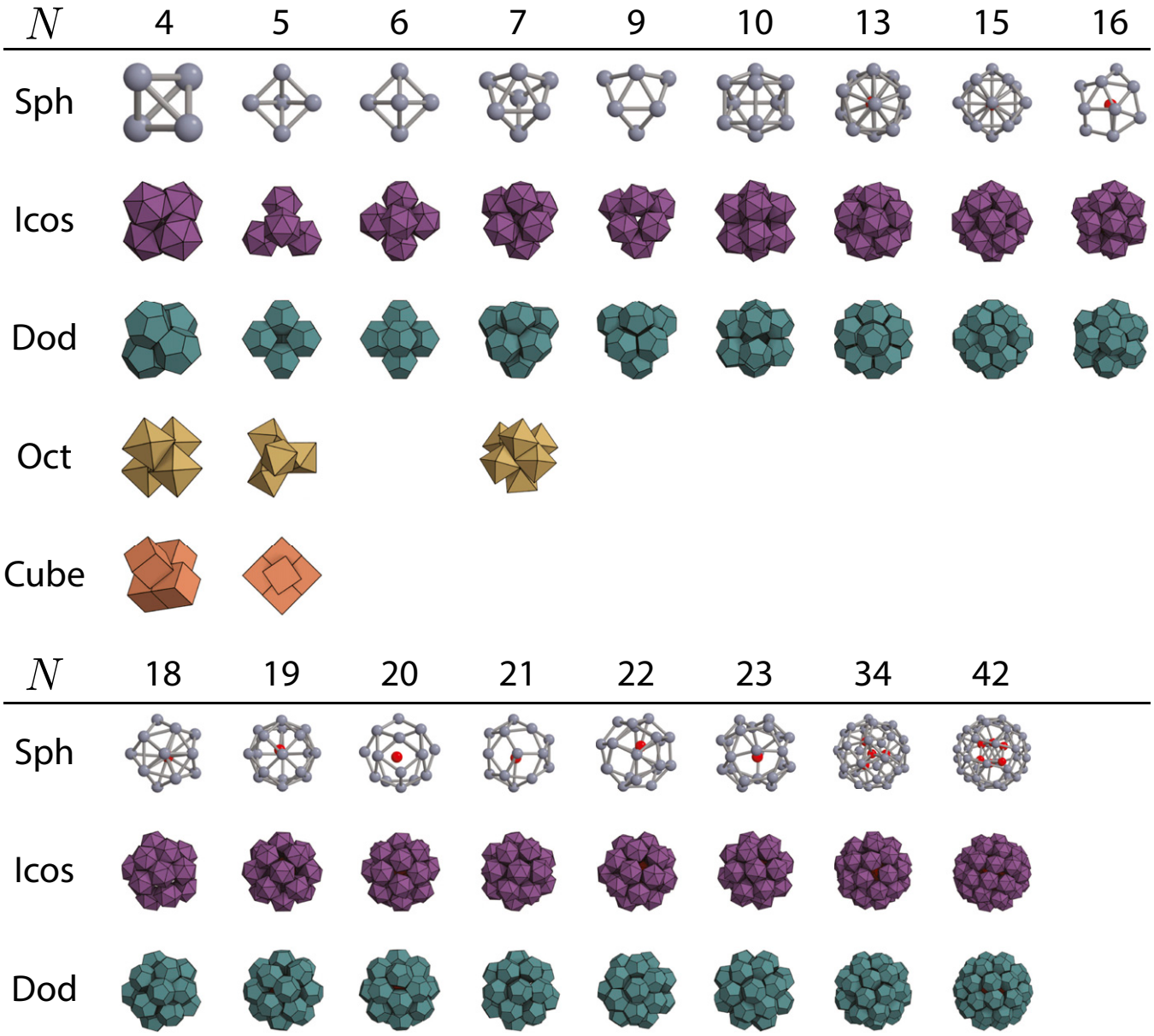

Fig. 3. Common cluster structures across multiple particle types. N indicates the number of particles in each cluster, and rows labeled Sph show the positions of the centroids of the corresponding sphere clusters. Rows labeled Icos, Dod, Oct, and Cube show corresponding clusters of icosahedra, dodecahedra, octahedra, and cubes, respectively. Clusters of Platonic solids are similar to these sphere clusters, and included in this table, if $M_{dist}^{sph} > 0.88$. At $N = 5$ the sphere, dodecahedron, and cube clusters are a square pyramid, whereas the icosahedron and octahedron clusters are the $N = 5$ optimal spherical code, a triangular bipyramid.

Magic Numbers. In every density profile the cluster density jumps at certain values of N and is markedly larger than densities at $N-1$ and $N+1$. These values of N are marked by gray circles in Fig. 4; we term them "magic numbers" in deference to the wealth of literature exploring magic numbers in other cluster systems. Typically, magic numbers in these systems correspond to clusters of minimal energy (78, 79, 81, 99–101).

We deem a cluster at N to be a magic-number cluster if its density ϕ_{circ}^{N} meets three criteria:

i) $\Delta\phi_{circ}^{N} \equiv \phi_{circ}^{N} - \frac{1}{2}(\phi_{circ}^{N-1} + \phi_{circ}^{N+1}) > 0.009$
ii) $\phi_{circ}^{N} > \phi_{circ}^{N-1}$
iii) $\phi_{circ}^{N} > \phi_{circ}^{N+1}$

Clusters at $N = 4$ and $N = 60$, the minimum and maximum values of N, are not considered, because they are incapable of satisfying criterion *i* and criterion *ii* or *iii*, respectively. The cutoff value of 0.009 delimits a varied sample of clusters drawn from every particle shape that nevertheless represents only a small fraction (~ 0.064) of all generated clusters. See the *SI Appendix* for more details.

The magic-number clusters for all particle shapes are shown in Fig. 5, along with the symmetry point groups of their layers. The structure and symmetry of each magic-number cluster vary widely both with N and particle shape.

Magic-number clusters of spheres, icosahedra, and dodecahedra consist of either a single layer or a central single particle or dimer surrounded by an outer layer that maps to an optimal spherical code in 12 out of 15 cases. Multiple shapes have the same outer-layer structure at $N = 6$, 12 and 13, 21, and 38. Note that the $N = 25$ sphere and dodecahedron clusters do not actually

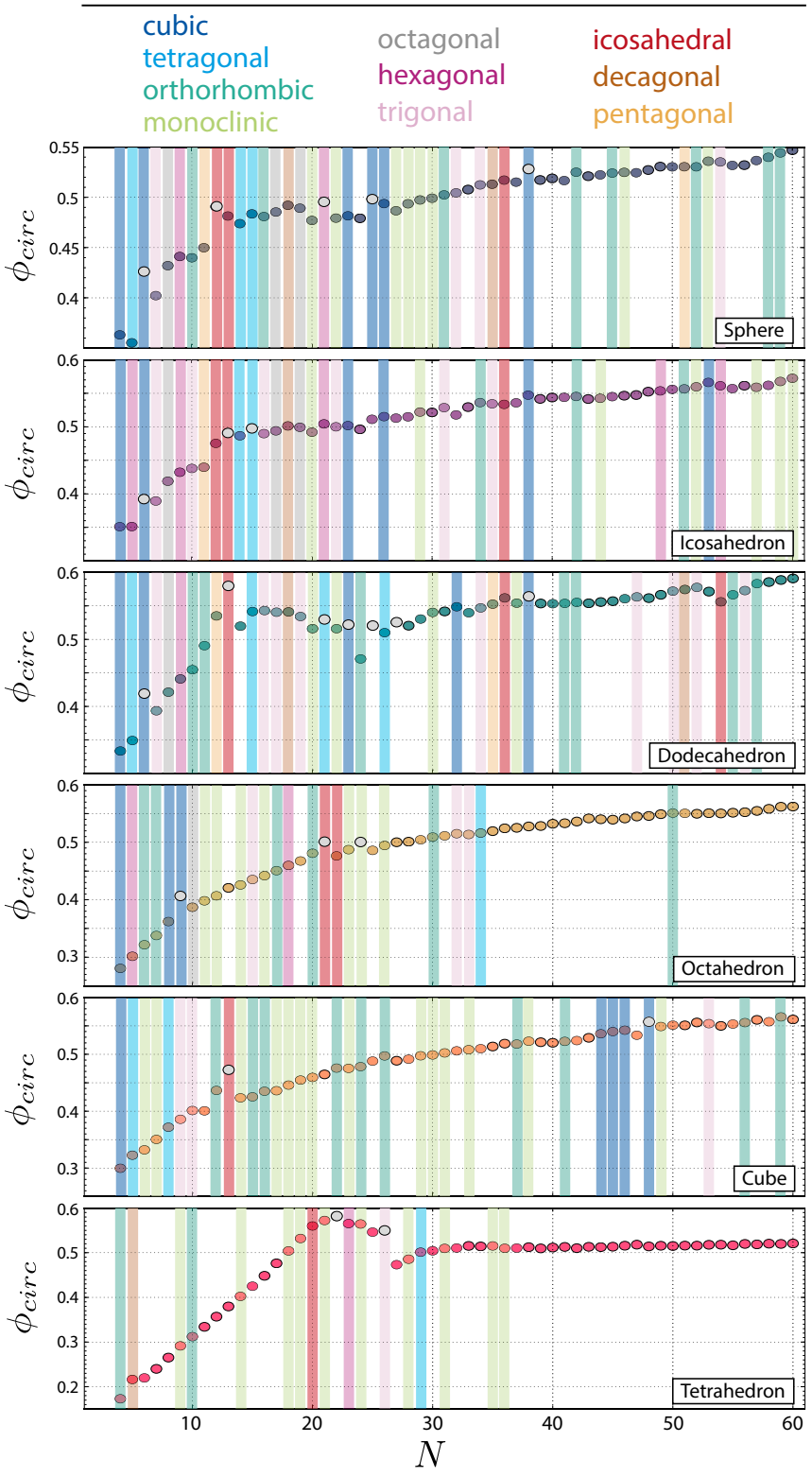

Fig. 4. ϕ_{circ} with respect to particle number for all densest clusters found. Colored bars indicate the crystal system of each outer cluster layer. Identically colored bars for clusters of different shapes denote the same crystal system. Gray data points are those deemed to be magic-number clusters.

share the same structure; the sphere cluster is a central particle surrounded by the $N=24$ optimal spherical code, whereas the dodecahedron cluster is a central dimer surrounded by the $N=23$ optimal spherical code. Of the three magic-number clusters that are not layers of optimal spherical codes ($N=27$ dodecahedra, $N=38$ spheres, and $N=38$ dodecahedra), the case of $N=38$ spheres and dodecahedra is particularly interesting. These clusters are both slight distortions of a particular common structure, a central six-particle octahedron surrounded by an outer layer whose centroids make up the union of a truncated octahedron and a

Table 2. Crystal systems of all outer cluster layers

Crystal system	Sphere	Icosahedron	Dodecahedron	Octahedron	Cube	Tetrahedron
Cubic	6	6	5	3	5	0
Hexagonal	2	5	1	2	0	1
Trigonal	4	6	9	3	3	1
Tetragonal	3	2	4	1	2	1
Orthorhombic	8	3	7	6	10	2
Monoclinic	8	7	4	7	14	10
Icosahedral	3	3	3	2	1	1
Decagonal	2	1	2	0	0	1
Octagonal	3	3	1	1	0	0
Pentagonal	2	1	2	0	0	0
Total	41	37	38	25	35	17

For each particle shape, data show the total number of outer layers whose symmetry point group belongs to each crystal system. A blank row separates crystal systems that are crystallographic from those that are not.

cube. (See Fig. 5 for an illustration. The $N = 38$ icosahedron cluster is also observed to share this structure, although it is not a magic-number cluster and its value of M_{dist}^{sph} is only ~ 0.77.) Although its outer layer is not an optimal spherical code, the $N = 38$ motif occupies a unique place in the pantheon of sphere cluster literature. It is an especially spherical arrangement of maximally close-packed spheres and is thus optimal under a range of circumstances beyond just dense packing inside a spherical container. The undistended version of this cluster is a segment of the *fcc* sphere packing, the densest packing possible for spheres in the bulk limit. Called the *fcc* truncated octahedron, this cluster is additionally known to be the global energy minimum of the 38-atom Lennard-Jones cluster (100, 102–104).

The magic-number clusters of the octahedra, cubes, and tetrahedra do not resemble optimal spherical codes, but rather are unique configurations whose structures allow each set of particles to be reasonably spherical and tightly packed. All magic-number clusters are displayed in Fig. 5; only a portion will be discussed here. The $N = 9$ octahedron cluster is a central particle surrounded by eight others, each face-sharing with it, in a regular cubic configuration. The $N = 21$ octahedron cluster is a central particle surrounded by a cage of 20 others, face-sharing with each other, in a regular dodecahedral configuration. The $N = 13$ cube cluster is an irregular icosahedral configuration surrounding a central particle in six sets of face-to-face aligned dimers. (A regular icosahedral configuration is an optimal spherical code, but the particular arrangement of these dimers distorts the configuration such that M_{dist}^{SC} does not register the similarity.) The $N = 48$ cube cluster consists of the $N = 13$ cluster, with one dimer replaced by a single particle, surrounded by an outer layer of 36 particles with cubic symmetry (six particles per cubic "side").

One notable surprise occurs for tetrahedra and suggests a connection between dense packings in a sphere and locally preferred motifs (105) during the self-assembly of an unconfined bulk system. A bulk fluid of tetrahedra self-assembles into a dodecagonal quasicrystal under suitable conditions (106), forming a structure that is markedly different from the bulk densest known packing of tetrahedra [a crystalline arrangement with four tetrahedra per unit cell, arranged in two face-sharing dimers (63)]. It was shown that en route to the quasicrystal, 20-tetrahedron icosahedral clusters in the fluid rearrange to form a 22-tetrahedron structure (106). This 22-tetrahedron cluster consists of two pentagonal dipyramids at the cluster poles and a set of six face-to-face aligned dimers ringing the cluster equator. It is precisely the structure we find to be a magic-number cluster. Indeed, our set of densest found tetrahedron clusters forms a telling sequence of structures: as N increases, the densest cluster passes from the $N = 5$ pentagonal dipyramid, through the $N = 20$ icosahedron, and maximizes cluster density at $N = 22$. Cluster density then dips, and significantly drops at $N = 27$ when the densest found cluster contains a particle at its center. That the $N = 22$ tetrahedron cluster is both a prominent motif in the self-assembled quasicrystal and the densest structure inside a sphere for $N = (4 - 60)$ suggests that the self-assembly of tetrahedra may favor the formation of local structures that pack densely inside a sphere.

Magic-number structures are unique, but all exhibit a trade-off between face-to-face alignment among particles, which enables tight packing but not necessarily cluster sphericity, and other types of contact between particles, which may promote cluster sphericity but not tight packing. No single rule seems to determine what makes a particular cluster "magic" for any particle shape: locally maximal density does not select for a particular type of symmetry or structure across particle types or even within the same particle type. These magic-number clusters do, however, provide a set of especially dense structures that possess symmetries not achievable via the spherical confinement of spheres, icosahedra, or dodecahedra at identical values of N, a fact whose implications will be discussed in the following section.

Conclusions

We generated finite dense packings of the Platonic solids, for $N = (4 - 60)$ constituent particles, using Monte Carlo sampling within spherical confinement. We found that generated packings were layered structures, possessing maximally three layers at high N and displaying a variety of point groups. Packings of the more spherical icosahedra and dodecahedra were structurally similar to sphere packings generated by the same method for many values of N, whereas packings of octahedra and cubes were similar to sphere packings only in two instances each, and packings of tetrahedra never matched sphere packings. Common packing structures were layers of optimal spherical codes in a majority of cases. The widespread similarity of finite dense packings of icosahedra and dodecahedra inside a spherical container to those of spheres indicates the suppression of the packing effects of particle shape by the container. Rather than particle shape and orientation, it is the particles' ability to pack tightly into spherical shells by mimicking the behavior of spherical particles and forming optimal spherical codes that enables dense packing. This is a result in contrast to dense packing in infinite 3D Euclidean space, for which particle shape strongly influences packing structure (60, 62, 65).

We also generated cluster density profiles across N for each particle shape and noted that spheres were not the worst packers

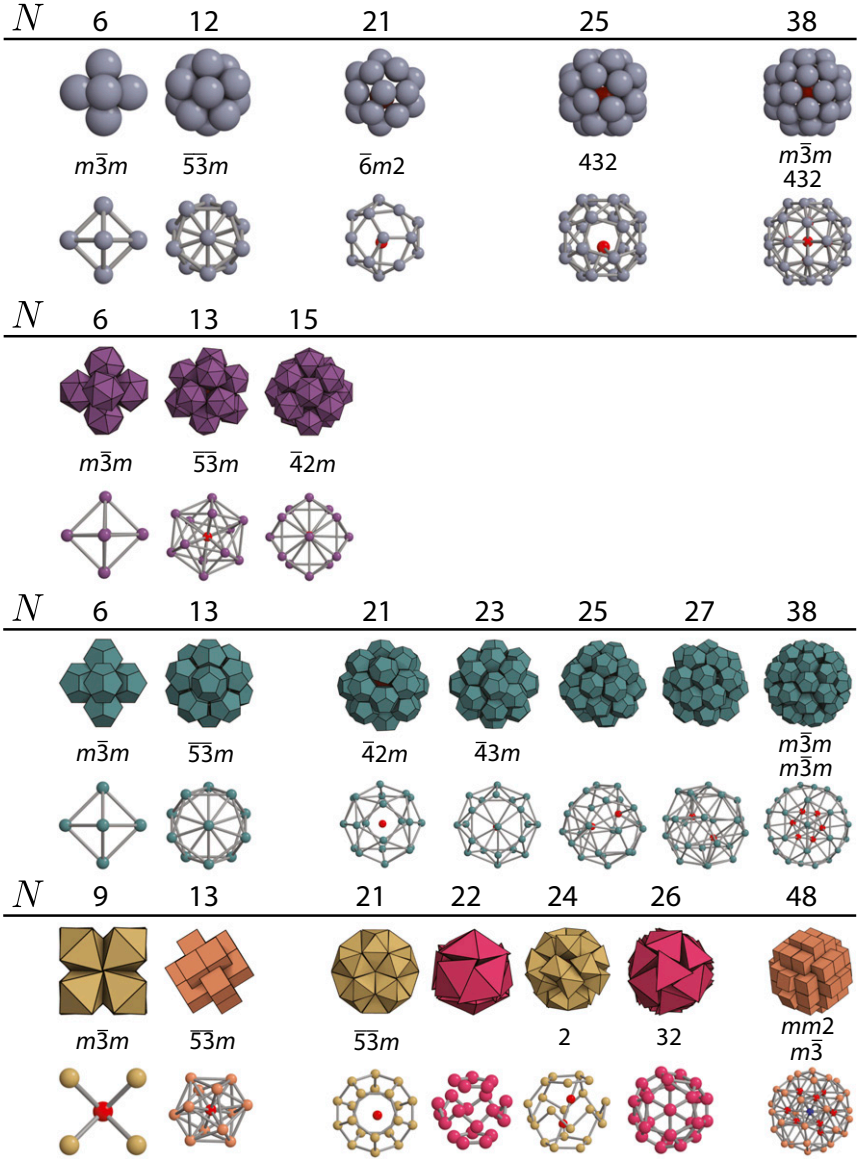

Fig. 5. All magic-number clusters for the spheres and polyhedra studied. Headers above each row of images show the particle number *N* of each cluster. Cluster snapshots and centroid skeletons are shown. Included with each set of cluster images are the symmetry point groups of its layers. When multiple symmetries are shown, the topmost symmetry belongs to the inner cluster layer.

with respect to the volume of the container at most values of *N*, and were in fact the best packers at especially low values of *N*. This result is not consistent with the conjectured behavior of dense packings of spheres and convex solids in infinite space (97); we hypothesize that it is due to the fact that spheres pack more densely than faceted convex particles near the surface of a spherical container. This surface packing effect becomes less influential on density as system size increases. Our density profiles additionally indicated clusters of especially dense design that we termed magic-number clusters. These clusters vary in symmetry and structure.

Common structures shared by clusters of spheres, icosahedra, dodecahedra, and in a few cases octahedra and even cubes are a class of dense motifs that are resistant to changes in particle shape, a result of interest to those in the colloidal and plasmonics communities for whom the fabrication of highly spherical particles is difficult to achieve or experimentally undesirable. In the plasmonics community, for example, recent efforts have focused on the manufacture of highly spherical metallic nanoparticles for the production of plasmonic nanoclusters with consistent and reproducible structure (77). However, faceted geometries are thermodynamically preferred over spherical geometries during the metallic nanoparticle growth process (77, 107), which complicates the production of spherical metallic nanoparticles. We showed here that a host of sphere cluster geometries, including among many others the optically interesting four-particle tetrahedron (27) and 13-particle centered icosahedron (108), are in fact robust against changes in particle shape. They can be formed by significantly nonspherical particles if the clusters are created via spherical confinement. Moreover, faceted particles within these common motifs assume a variety of contacts with their neighbors, including edge-to-edge, face-to-face, and edge-to-face. Recent work on the optical properties of different metallic nanoparticle junction types (31, 33) indicates that our clusters, although they share common geometries, may exhibit diverse and interesting optical behavior if formed from metallic nanoparticles.

Our dense magic-number clusters provide examples of structures with experimentally useful geometries that are difficult to

achieve otherwise. Many magic-number clusters, especially of the less spherical shapes, have configurations that are not achievable by densely packing spheres, and could be accessible via confinement within an emulsion droplet or other spherical container. For instance, our densest cluster of 21 octahedra, a dodecahedral cage of 20 particles surrounding a central one, possesses a structure that closely packed spheres, either within a spherical container or in bulk, do not adopt. Moreover, recent work shows that this dodecahedral geometry may have implications for self-assembled metamaterials (109).

Other classes of packing in confinement problems are compelling future subjects of investigation. For example, confining geometries beyond spheres are frequently leveraged in the laboratory, including cylinders and cylindrical wells (33, 110–112), rectilinear channels (33, 110, 113, 114), and the space near planar walls (35, 115, 116). Another set of packing in confinement problems, for which the packing object is a flexible or semiflexible polymer rather than a particle, is related to the containment of genomic material in cells and virus capsids. This confinement is conjectured to influence gene expression and regulation (3, 4), ordering of the genome into spool-like, toroidal, or liquid-crystalline structures (4, 117, 118), and ejection of the genome from virus capsids into other cells (117, 118). Countless studies, inspired by the ubiquity of biopolymer packing in confinement, have investigated polymer behavior inside spheres and rod-like containers (119, 120), in boxes (121), in slit-like channels and tubes (122, 123), in quasi-2D confinement (124), and even on curved 2D surfaces (125). Recently, ellipsoid packing and assembly in spherical and ellipsoidal confinement (56, 58, 126) has been used to mimic the effects of cell nucleus confinement on the behavior of ellipsoid-like nucleosomes and higher-order chromosome territories (3, 127, 128). The richness of our results for polyhedra in spherical confinement suggests that further investigation into the interplay between particle shape and container shape in these new packing in confinement problems will be interesting and informative.

ACKNOWLEDGMENTS. We thank M. E. Irrgang, B. Schultz, J. Proctor, P. Damasceno, X. Du, and R. Newman for innumerable fruitful discussions. This work was supported by US Army Research Office Grant W911NF-10-1-0518 (to S.C.G. and G.v.A.), National Science Foundation Graduate Research Fellowship Grant DGE 1256260 (to E.G.T.), FP7 Marie Curie Actions of the European Commission Grant PIOF-GA-2011-302490 Actsa (to D.K.), and an Early Postdoc.Mobility Fellowship from Swiss National Science Foundation Grant P2EZP2_152128 (to J.D.). This research was supported in part through computational resources and services supported by Advanced Research Computing at the University of Michigan, Ann Arbor. This work also used the Extreme Science and Engineering Discovery Environment (XSEDE), which is supported by National Science Foundation Grant ACI-1053575, XSEDE Award DMR 140129.

1. Balbo J, Mereghetti P, Herten DP, Wade RC (2013) The shape of protein crowders is a major determinant of protein diffusion. *Biophys J* 104(7):1576–1584.
2. Ellis RJ (2001) Macromolecular crowding: Obvious but underappreciated. *Trends Biochem Sci* 26(10):597–604.
3. Cremer T, Cremer C (2001) Chromosome territories, nuclear architecture and gene regulation in mammalian cells. *Nat Rev Genet* 2(4):292–301.
4. Marenduzzo D, Micheletti C, Orlandini E (2010) Biopolymer organization upon confinement. *J Phys Condens Matter* 22(28):283102.
5. Åström JA, Karttunen M (2006) Cell aggregation: Packing soft grains. *Phys Rev E* 73(6):062301.
6. Hayashi T, Carthew RW (2004) Surface mechanics mediate pattern formation in the developing retina. *Nature* 431(7009):647–652.
7. Cines DB, et al. (2014) Clot contraction: Compression of erythrocytes into tightly packed polyhedra and redistribution of platelets and fibrin. *Blood* 123(10):1596–1603.
8. Hifi M, M'Hallah R (2009) A literature review on circle and sphere packing problems: Models and methodologies. *Adv Oper Res* 2009:150624.
9. Wäscher G, Haußner H, Schumann H (2007) An improved typology of cutting and packing problems. *Eur J Oper Res* 183(3):1109–1130.
10. van Blaaderen A (2003) Colloidal molecules and beyond. *Science* 301(5632):470–471.
11. Wang Y, et al. (2012) Colloids with valence and specific directional bonding. *Nature* 491(7422):51–55.
12. Phillips CL, et al. (2014) Digital colloids: Reconfigurable clusters as high information density elements. *Soft Matter* 10(38):7468–7479.
13. Dinsmore AD, et al. (2002) Colloidosomes: Selectively permeable capsules composed of colloidal particles. *Science* 298(5595):1006–1009.
14. Velev OD, Lenhoff AM, Kaler EW (2000) A class of microstructured particles through colloidal crystallization. *Science* 287(5461):2240–2243.
15. Manoharan VN, Elsesser MT, Pine DJ (2003) Dense packing and symmetry in small clusters of microspheres. *Science* 301(5632):483–487.
16. Klein SM, Manoharan VN, Pine DJ, Lange FF (2005) Synthesis of spherical polymer and titania photonic crystallites. *Langmuir* 21(15):6669–6674.
17. Cho YS, et al. (2005) Self-organization of bidisperse colloids in water droplets. *J Am Chem Soc* 127(45):15968–15975.
18. Elsesser MT, Hollingsworth AD, Edmond KV, Pine DJ (2011) Large core-shell poly(methyl methacrylate) colloidal clusters: Synthesis, characterization, and tracking. *Langmuir* 27(3):917–927.
19. de Nijs B, et al. (2015) Entropy-driven formation of large icosahedral colloidal clusters by spherical confinement. *Nat Mater* 14(1):56–60.
20. Guzowski J, Garstecki P (2015) Droplet clusters: Exploring the phase space of soft mesoscale atoms. *Phys Rev Lett* 114(18):188302.
21. Liz-Marzán LM (2006) Tailoring surface plasmons through the morphology and assembly of metal nanoparticles. *Langmuir* 22(1):32–41.
22. Noguez C (2007) Surface plasmons on metal nanoparticles: The influence of shape and physical environment. *J Phys Chem C* 111(10):3806–3819.
23. Pendry JB, Schurig D, Smith DR (2006) Controlling electromagnetic fields. *Science* 312(5781):1780–1782.
24. De Angelis F, et al. (2008) A hybrid plasmonic-photonic nanodevice for label-free detection of a few molecules. *Nano Lett* 8(8):2321–2327.
25. Fang N, Lee H, Sun C, Zhang X (2005) Sub-diffraction-limited optical imaging with a silver superlens. *Science* 308(5721):534–537.
26. Klein MW, Enkrich C, Wegener M, Linden S (2006) Second-harmonic generation from magnetic metamaterials. *Science* 313(5786):502–504.
27. Urzhumov YA, et al. (2007) Plasmonic nanoclusters: A path towards negative-index metafluids. *Opt Express* 15(21):14129–14145.
28. Sheikholeslami SN, Alaeian H, Koh AL, Dionne JA (2013) A metafluid exhibiting strong optical magnetism. *Nano Lett* 13(9):4137–4141.
29. Urban AS, et al. (2013) Three-dimensional plasmonic nanoclusters. *Nano Lett* 13(9):4399–4403.
30. Schuller JA, et al. (2010) Plasmonics for extreme light concentration and manipulation. *Nat Mater* 9(3):193–204.
31. Gao B, Arya G, Tao AR (2012) Self-orienting nanocubes for the assembly of plasmonic nanojunctions. *Nat Nanotechnol* 7(7):433–437.
32. Rosen DA, Tao AR (2014) Modeling the optical properties of bowtie antenna generated by self-assembled Ag triangular nanoprisms. *ACS Appl Mater Interfaces* 6(6):4134–4142.
33. Henzie J, Andrews SC, Ling XY, Li Z, Yang P (2013) Oriented assembly of polyhedral plasmonic nanoparticle clusters. *Proc Natl Acad Sci USA* 110(17):6640–6645.
34. Kalpaxis P, Rickayzen G (1993) Structure of a confined fluid of hard ellipsoids. *Mol Phys* 80(2):391–406.
35. Henzie J, Grünwald M, Widmer-Cooper A, Geissler PL, Yang P (2012) Self-assembly of uniform polyhedral silver nanocrystals into densest packings and exotic superlattices. *Nat Mater* 11(2):131–137.
36. Camenen JF, Descantes Y, Richard P (2012) Effect of confinement on dense packings of rigid frictionless spheres and polyhedra. *Phys Rev E* 86(6):061317.
37. Marechal M, Löwen H (2013) Density functional theory for hard polyhedra. *Phys Rev Lett* 110(13):137801.
38. Thapar V, Hanrath T, Escobedo FA (2015) Entropic self-assembly of freely rotating polyhedral particles confined to a flat interface. *Soft Matter* 11(8):1481–1491.
39. Blachman NM (1963) The closest packing of equal spheres in a larger sphere. *Am Math Mon* 70(5):526–529.
40. Pickett GT, Gross M, Okuyama H (2000) Spontaneous chirality in simple systems. *Phys Rev Lett* 85(17):3652–3655.
41. Gensane T (2004) Dense packings of equal spheres in a cube. *Electron J Comb* 11(1):1–17.
42. Lauga E, Brenner MP (2004) Evaporation-driven assembly of colloidal particles. *Phys Rev Lett* 93(23):238301.
43. Chan HK (2011) Densest columnar structures of hard spheres from sequential deposition. *Phys Rev E* 84(5):050302.
44. Mughal A, Chan HK, Weaire D (2011) Phyllotactic description of hard sphere packing in cylindrical channels. *Phys Rev Lett* 106(11):115704.
45. M'Hallah R, Alkandari A, Mladenovic N (2013) Packing unit spheres into the smallest sphere using VNS and NLP. *Comput Oper Res* 40(2):603–615.
46. Wood DA, Santangelo CD, Dinsmore AD (2013) Self-assembly on a cylinder: A model system for understanding the constraint of commensurability. *Soft Matter* 9(42):10016.
47. Yamchi MZ, Bowles RK (2015) Helical defect packings in a quasi-one-dimensional system of cylindrically confined hard spheres. *Phys Rev Lett* 115(2):025702.
48. Artoni R, Richard P (2015) Effective wall friction in wall-bounded 3D dense granular flows. *Phys Rev Lett* 115(15):158001.
49. Hifi M, Yousef L, Zhou Z (2015) A dichotomous search-based heuristic for the three-dimensional sphere packing problem. *Cogent Eng* 2(1):994257.
50. Pfoertner H (2013) Densest packing of spheres in a sphere. Available at www.randomwalk.de/sphere/insphr/spheresinsphr.html. Accessed March 27, 2015.
51. Bennell J, Scheithauer G, Stoyan Y, Romanova T (2010) Tools of mathematical modeling of arbitrary object packing problems. *Ann Oper Res* 179(1):343–368.
52. Gensane T, Honvault P (2012) Optimal packings of two ellipses in a square. *Forum Geom* 14:371–380.

53. Galiev SI, Lisafina MS (2013) Numerical optimization methods for packing equal orthogonally oriented ellipses in a rectangular domain. *Comput Math Math Phys* 53(11):1748–1762.
54. Kallrath J, Rebennack S (2014) Cutting ellipses from area-minimizing rectangles. *J Glob Optim* 59(2):405–437.
55. Honvault P (2015) About the density of optimal packings of ellipses in a square. Technical report 517 (Les Cahiers du Laboratoire de Mathematiques Pures et Appliquées Joseph Liouville, Calais, France).
56. Uhler C, Wright SJ (2013) Packing ellipsoids with overlap. *SIAM Rev* 55(4):671–706.
57. Kallrath J (2015) Packing ellipsoids into volume-minimizing rectangular boxes. *J Glob Optim*, 10.1007/s10898-015-0348-6.
58. Birgin EG, Lobato RD, Martínez JM (2015) Packing ellipsoids by nonlinear optimization. *J Glob Optim*, 10.1007/s10898-015-0395-z.
59. Gensane T, Ryckelynck P (2008) Producing dense packings of cubes. *Discrete Math* 308(22):5230–5245.
60. Betke U, Henk M (1999) Densest lattice packings of 3-polytopes. *Comput Geom* 16(3):157–186.
61. Donev A, et al. (2004) Improving the density of jammed disordered packings using ellipsoids. *Science* 303(5660):990–993.
62. Torquato S, Jiao Y (2009) Dense packings of the Platonic and Archimedean solids. *Nature* 460(7257):876–879.
63. Chen ER, Engel M, Glotzer SC (2010) Dense crystalline dimer packings of regular tetrahedra. *Discrete Comput Geom* 44(2):253–280.
64. de Graaf J, van Roij R, Dijkstra M (2011) Dense regular packings of irregular nonconvex particles. *Phys Rev Lett* 107(15):155501.
65. Chen ER, Klotsa D, Engel M, Damasceno PF, Glotzer SC (2014) Complexity in surfaces of densest packings for families of polyhedra. *Phys Rev X* 4(1):011024.
66. Ahmadi TS, Wang ZL, Green TC, Henglein A, El-Sayed MA (1996) Shape-controlled synthesis of colloidal platinum nanoparticles. *Science* 272(5270):1924–1925.
67. Song H, Kim F, Connor S, Somorjai GA, Yang P (2005) Pt nanocrystals: Shape control and Langmuir-Blodgett monolayer formation. *J Phys Chem B* 109(1):188–193.
68. Sau TK, Murphy CJ (2004) Room temperature, high-yield synthesis of multiple shapes of gold nanoparticles in aqueous solution. *J Am Chem Soc* 126(28):8648–8649.
69. Tao AR, Habas S, Yang P (2008) Shape control of colloidal metal nanocrystals. *Small* 4(3):310–325.
70. Habas SE, Lee H, Radmilovic V, Somorjai GA, Yang P (2007) Shaping binary metal nanocrystals through epitaxial seeded growth. *Nat Mater* 6(9):692–697.
71. Fan FR, et al. (2008) Epitaxial growth of heterogeneous metal nanocrystals: From gold nano-octahedra to palladium and silver nanocubes. *J Am Chem Soc* 130(22): 6949–6951.
72. Seo D, Park JC, Song H (2006) Polyhedral gold nanocrystals with O_h symmetry: From octahedra to cubes. *J Am Chem Soc* 128(46):14863–14870.
73. Demortière A, Launois P, Goubet N, Albouy PA, Petit C (2008) Shape-controlled platinum nanocubes and their assembly into two-dimensional and three-dimensional superlattices. *J Phys Chem B* 112(46):14583–14592.
74. Rossi L, et al. (2011) Cubic crystals from cubic colloids. *Soft Matter* 7(9):4139–4142.
75. Zhang J, et al. (2012) Reversible Kirkwood-Alder transition observed in Pt_3Cu_2 nanoctahedron assemblies under controlled solvent annealing/drying conditions. *J Am Chem Soc* 134(34):14043–14049.
76. Xia Y, Xia X, Wang Y, Xie S (2013) Shape-controlled synthesis of metal nanocrystals. *MRS Bull* 38:335–344.
77. Lee YJ, et al. (2013) Ultrasmooth, highly spherical monocrystalline gold particles for precision plasmonics. *ACS Nano* 7(12):11064–11070.
78. Echt O, Sattler K, Recknagel E (1981) Magic numbers for sphere packings: Experimental verification in free xenon clusters. *Phys Rev Lett* 47(16):1121–1124.
79. Beck TL, Jellinek J, Berry RS (1987) Rare gas clusters: Solids, liquids, slush, and magic numbers. *J Chem Phys* 87(1):545–554.
80. Doye JP, Wales DJ (1995) Magic numbers and growth sequences of small face-centered-cubic and decahedral clusters. *Chem Phys Lett* 247(4):339–347.
81. Chen T, Zhang Z, Glotzer SC (2007) A precise packing sequence for self-assembled convex structures. *Proc Natl Acad Sci USA* 104(3):717–722.
82. Frenkel D, Smit B (2002) *Understanding Molecular Simulation: From Algorithms to Applications* (Academic, San Diego), 2nd Ed, p 118.
83. Damasceno PF, Engel M, Glotzer SC (2012) Predictive self-assembly of polyhedra into complex structures. *Science* 337(6093):453–457.
84. Osserman R (1978) The isoperimetric inequality. *Bull Am Math Soc* 84(6):1182–1239.
85. Ester M, Kriegel H, Sander J, Xu X (1996) A density-based algorithm for discovering clusters in large spatial databases with noise. *Proceedings of the Second International Conference on Knowledge Discovery and Data Mining* (AAAI, Portland, OR), pp 226–231.
86. Pedregosa F, et al. (2011) Scikit-learn: Machine learning in python. *J Mach Learn Res* 12:2825–2830.
87. Steinhardt PJ, Nelson DR, Ronchetti M (1983) Bond-orientational order in liquids and glasses. *Phys Rev B* 28(2):784–805.
88. Keys AS, Iacovella CR, Glotzer SC (2011) Characterizing complex particle morphologies through shape matching: Descriptors, applications, and algorithms. *J Comput Phys* 230(17):6438–6463.
89. Conway JH, Sloane N (1999) *Sphere Packings, Lattices and Groups* (Springer, New York), 3rd Ed, pp 97–98.
90. Hopkins AB, Stillinger FH, Torquato S (2010) Spherical codes, maximal local packing density, and the golden ratio. *J Math Phys* 51(4):043302.
91. Hopkins AB, Stillinger FH, Torquato S (2011) Densest local sphere-packing diversity. II. Application to three dimensions. *Phys Rev E* 83(1):011304.
92. Sloane N (2015) Spherical codes. Available at neilsloane.com/packings/. Accessed March 31, 2015.
93. Damasceno PF, Engel M, Glotzer SC (2012) Crystalline assemblies and densest packings of a family of truncated tetrahedra and the role of directional entropic forces. *ACS Nano* 6(1):609–614.
94. Gantapara AP, de Graaf J, van Roij R, Dijkstra M (2013) Phase diagram and structural diversity of a family of truncated cubes: Degenerate close-packed structures and vacancy-rich states. *Phys Rev Lett* 111(1):015501.
95. Kottwitz D (1991) The densest packing of equal circles on a sphere. *Acta Crystallogr A* 47(3):158–165.
96. Phillips CL, Jankowski E, Marval M, Glotzer SC (2012) Self-assembled clusters of spheres related to spherical codes. *Phys Rev E* 86(4):041124.
97. Gardner M (2001) *The Colossal Book of Mathematics: Classic Puzzles, Paradoxes, and Problems* (Norton, New York), 1st Ed, p 135.
98. Kallus Y (2014) The 3-ball is a local pessimum for packing. *Adv Math* 264:355–370.
99. Harris IA, Kidwell RS, Northby JA (1984) Structure of charged argon clusters formed in a free jet expansion. *Phys Rev Lett* 53(25):2390–2393.
100. Doye JPK, Wales DJ, Berry RS (1995) The effect of the range of the potential on the structures of clusters. *J Chem Phys* 103(10):4234–4249.
101. Doye JPK, Wales DJ (2001) Polytetrahedral clusters. *Phys Rev Lett* 86(25):5719–5722.
102. Pillardy J, Piela L (1995) Molecular dynamics on deformed potential energy hypersurfaces. *J Phys Chem* 99(31):11805–11812.
103. Barrón C, Gómez S, Romero D (1996) Archimedean polyhedron structure yields a lower energy atomic cluster. *Appl Math Lett* 9(5):75–78.
104. Doye JPK, Miller MA, Wales DJ (1999) The double-funnel energy landscape of the 38-atom Lennard-Jones cluster. *J Chem Phys* 110(14):6896–6906.
105. van Anders G, Klotsa D, Ahmed NK, Engel M, Glotzer SC (2014) Understanding shape entropy through local dense packing. *Proc Natl Acad Sci USA* 111(45):E4812–E4821.
106. Haji-Akbari A, et al. (2009) Disordered, quasicrystalline and crystalline phases of densely packed tetrahedra. *Nature* 462(7274):773–777.
107. Millstone JE, Hurst SJ, Métraux GS, Cutler JI, Mirkin CA (2009) Colloidal gold and silver triangular nanoprisms. *Small* 5(6):646–664.
108. Fontana J, et al. (2014) Virus-templated plasmonic nanoclusters with icosahedral symmetry via directed self-assembly. *Small* 10(15):3058–3063.
109. Fruhnert M, Mühlig S, Lederer F, Rockstuhl C (2014) Towards negative index self-assembled metamaterials. *Phys Rev B* 89(7):075408.
110. Yin Y, Lu Y, Gates B, Xia Y (2001) Template-assisted self-assembly: A practical route to complex aggregates of monodispersed colloids with well-defined sizes, shapes, and structures. *J Am Chem Soc* 123(36):8718–8729.
111. Li F, Badel X, Linnros J, Wiley JB (2005) Fabrication of colloidal crystals with tubular-like packings. *J Am Chem Soc* 127(10):3268–3269.
112. Fan JA, et al. (2012) Plasmonic mode engineering with templated self-assembled nanoclusters. *Nano Lett* 12(10):5318–5324.
113. Vanapalli SA, et al. (2008) Fluidic assembly and packing of microspheres in confined channels. *Langmuir* 24(7):3661–3670.
114. Harth K, Mauney A, Stannarius R (2015) Frustrated packing of spheres in a flat container under symmetry-breaking bias. *Phys Rev E* 91(3):030201.
115. Neser S, Bechinger C, Leiderer P, Palberg T (1997) Finite-size effects on the closest packing of hard spheres. *Phys Rev Lett* 79(12):2348–2351.
116. Royall CP, Dzubiella J, Schmidt M, van Blaaderen A (2007) Nonequilibrium sedimentation of colloids on the particle scale. *Phys Rev Lett* 98(18):188304.
117. Kindt J, Tzlil S, Ben-Shaul A, Gelbart WM (2001) DNA packaging and ejection forces in bacteriophage. *Proc Natl Acad Sci USA* 98(24):13671–13674.
118. Leforestier A, Livolant F (2010) The bacteriophage genome undergoes a succession of intracapsid phase transitions upon DNA ejection. *J Mol Biol* 396(2):384–395.
119. Jun S, Mulder B (2006) Entropy-driven spatial organization of highly confined polymers: Lessons for the bacterial chromosome. *Proc Natl Acad Sci USA* 103(33): 12388–12393.
120. Oskolkov NN, Linse P, Potemkin II, Khokhlov AR (2011) Nematic ordering of polymers in confined geometry applied to DNA packaging in viral capsids. *J Phys Chem B* 115(3):422–432.
121. Fritsche M, Heermann DW (2011) Confinement driven spatial organization of semiflexible ring polymers: Implications for biopolymer packaging. *Soft Matter* 7(15):6906–6913.
122. Brochard F, de Gennes PG (1977) Dynamics of confined polymer chains. *J Chem Phys* 67(1):52–56.
123. Chrissopoulou K, Anastasiadis SH (2015) Effects of nanoscopic-confinement on polymer dynamics. *Soft Matter* 11(19):3746–3766.
124. Soares e Silva M, et al. (2011) Self-organized patterns of actin filaments in cell-sized confinement. *Soft Matter* 7(22):10631–10641.
125. Lin CH, Tsai YC, Hu CK (2007) Wrapping conformations of a polymer on a curved surface. *Phys Rev E* 75(3):031903.
126. Saper G, et al. (2013) Effect of capsid confinement on the chromatin organization of the SV40 minichromosome. *Nucleic Acids Res* 41(3):1569–1580.
127. Bolzer A, et al. (2005) Three-dimensional maps of all chromosomes in human male fibroblast nuclei and prometaphase rosettes. *PLoS Biol* 3(5):e157.
128. Khalil A, et al. (2007) Chromosome territories have a highly nonspherical morphology and nonrandom positioning. *Chromosome Res* 15(7):899–916.